



Article

Crystal-Chemical Evolution of Muscovite and Nb-Ta-Y-REE-Bearing Minerals in the Wadi Al-Baroud Granite-Pegmatite System

Mabrouk Sami ^{1,*}, Ioan V. Sanislav ², Avish A. Kumar ², Mostafa R. Abukhadra ¹, Vandi Dlama Kamaunji ³

- Geosciences Department, College of Science, United Arab Emirates University, Al Ain 15551, United Arab Emirates; m.abdelwahab@uaeu.ac.ae
- ² Economic Geology Research Centre (EGRU), College of Science and Engineering, James Cook University, Townsville 4814, Australia
- School of Earth Sciences, China University of Geosciences, Wuhan 430074, China
- Geology and Geophysics Department, College of Science, King Saud University, P.O. Box 16 2455, Riyadh 11451, Saudi Arabia
- * Correspondence: mabrouksami@uaeu.ac.ae (M.S.); salhejji@ksu.edu.sa (S.S.A.)

Abstract

The Wadi Al-Baroud granite-pegmatite system in the Eastern Desert of Egypt displays a progressive rare-metal enrichment evident in the crystal chemistry of muscovite mica and associated Nb-Ta-Y-REE oxide minerals. EMP analyses demonstrate that pegmatite-hosted muscovite is systematically enriched in Si, Fe, Mg, and fluorine compared to its granitic counterpart, reflecting crystallization from volatile-rich, highly evolved melts. Columbite group minerals exhibit pronounced fractionation trends, with pegmatitic columbite showing Ta and Mn enrichment and a low Nb/Ta ratio, indicative of late-stage F- and H₂Orich melt evolution and advanced magmatic differentiation. Y-Nb-Ti oxides, especially fergusonite-Y and euxenite-Y, record exceptional enrichment in high-field-strength elements (HFSEs) and heavy rare earth elements (HREEs), further driven by structural focusing and fluid-mediated alteration. These crystal-chemical trends record an extreme fractional crystallization and magmatic-hydrothermal transition, wherein F-rich fluids modified early magmatic minerals and promoted the incorporation of Y, REEs, Th, and U into late-stage oxides. The data indicate a two-stage evolutionary model, in which rare-metal mineralization first occurred through primary magmatic crystallization within the granite, followed by fluid-driven re-equilibration in the pegmatites. This integrated mineral-chemical approach provides a clearer understanding of rare-metal enrichment processes in granite-pegmatite systems and offers refined criteria for identifying exploration targets for Nb, Ta, Y, and HREEs.

Keywords: rare-metal granites and pegmatites; columbite-group minerals; muscovite substitutions; crystal chemistry; fergusonite-euxenite; Eastern Desert; Egypt



Academic Editor: Manuel Munoz

Received: 1 October 2025 Revised: 9 November 2025 Accepted: 12 November 2025 Published: 16 November 2025

Citation: Sami, M.; Sanislav, I.V.; Kumar, A.A.; Abukhadra, M.R.; Kamaunji, V.D.; Alhejji, S.S. Crystal-Chemical Evolution of Muscovite and Nb-Ta-Y-REE-Bearing Minerals in the Wadi Al-Baroud Granite-Pegmatite System. *Minerals* 2025, 15, 1206. https://doi.org/ 10.3390/min15111206

Copyright: © 2025 by the authors. Licensee MDPI, Basel, Switzerland. This article is an open access article distributed under the terms and conditions of the Creative Commons Attribution (CC BY) license (https://creativecommons.org/licenses/by/4.0/).

1. Introduction

Rare-metal granites and their pegmatitic derivatives are critical sources of Nb, Ta, and rare earth elements (REEs) metals essential for high-technology applications. Their mineralogical and geochemical evolution is strongly governed by fractional crystallization, volatile enrichment, and various crystal-chemical substitution processes in both accessory and rock-forming minerals [1]. Among these minerals, muscovite, columbite-group

Minerals **2025**, 15, 1206 2 of 22

minerals (CGMs), and Y–Nb–Ti oxides serve as especially sensitive tracers of magmatic-hydrothermal processes. Their compositions record the interplay of substitution vectors, volatile complexation, and melt–fluid interaction, which collectively control the distribution of high-field-strength elements (HFSE) and REE in evolved felsic systems [2].

The Nubian Shield hosts a significant abundance of rare-metal-bearing granites and granitic pegmatites [1,3]. Pegmatites serve as primary sources of Sn and Ta in several countries, including Uganda, Rwanda, Burundi, and the Democratic Republic of the Congo, reflecting their importance in regional metallogeny. Specialized rare-metal granites and pegmatites across Egypt, Nigeria, Namibia, Mozambique, Zimbabwe, Ethiopia, South Africa, Somalia, and parts of West Africa constitute major provinces for Ta, Nb, and Sn mineralization [4,5]. Within the Arabian–Nubian Shield (ANS), particularly in Saudi Arabia and Egypt, rare-metal granites are recognized for their considerable economic potential. Specific world-class deposits, such as the Nuweibi and Abu Dabbab plutons in Egypt, as well as Al-Ghurayyah in Saudi Arabia, are projected to rank among the world's foremost Ta producers, potentially supplying up to 65% of the primary global output [6,7].

The role of volatiles, particularly fluorine, in driving extreme magmatic fractionation is well established. Fluorine lowers melt viscosity and solidus temperatures, prolongs crystallization, and forms stable complexes with HFSE and HREE, thereby enhancing their solubility in residual melts [8]. Consequently, fluorine-rich environments promote the crystallization of HREE- and Ta-enriched oxides and micas in late-stage pegmatites [9]. Simultaneously, crystal-chemical substitutions, such as the phengitic and ferrimuscovite exchanges in muscovite, and Mn–Fe–Nb–Ta partitioning in CGMs, record evolving redox states, temperature, and fluid–melt chemistry [10]. Thus, linking mineral chemistry to magmatic–fluid evolution provides a powerful framework for unraveling the metallogenic pathways of rare-metal provinces.

Despite the widespread occurrence of rare-metal pegmatites within granitic and metamorphic host rocks in Egyptian Eastern Desert, exemplified by occurrences at Gebel Abu Dob, El-Ineigi, Ras Baroud, Wadi Sikait, and Wadi Zareib [11,12], these systems need further investigation. Comprehensive studies addressing the crystal-chemical evolution of both rock-forming and accessory minerals, and their role in deciphering the magmatic-hydrothermal history of rare-metal granite-pegmatite systems, also remain limited [13]. The Eastern Desert of Egypt forms part of the ANS, where Pan-African granitic magmatism has a suite of rare-metal-bearing granites and pegmatites [2,14]. Among these, the Wadi Al-Baroud system hosts abundant Nb-Ta-Y-REE mineralization [11,12,15,16], yet the crystal-chemical mechanisms underlying its rare-metal enrichment remain poorly constrained. Previous studies have largely emphasized whole-rock geochemistry, petrogenesis, and the chemistry of a few selected minerals [11,12,15,16]. By contrast, comprehensive mineral-scale investigations targeting muscovite and the diverse Nb-Ta-Y-REE-bearing phases are lacking.

In this study, we present integrated mineral-chemical data for muscovite, CGMs, and Y–Nb–Ti oxides from the Wadi Al-Baroud granite and its associated pegmatites. Our aims are to: (1) evaluate the crystal-chemical substitution mechanisms that govern the compositions of these phases; (2) assess the role of volatiles, especially fluorine, in promoting fractionation and rare-metal enrichment; (3) investigate mineral-scale paragenesis and textural evolution, including deformation-assisted localization and post-magmatic alteration of muscovite and Nb–Y–REE oxides; and (4) reconstruct the magmatic–hydrothermal evolution of the granite–pegmatite system. By combining textural, geochemical, and substitutional evidence, we develop a coherent model for the rare-metal mineralization processes in this Pan-African terrane and place the Wadi Al-Baroud system in the broader context of global LCT (Li–Cs–Ta-type) pegmatite and rare-metal granite provinces.

Minerals 2025, 15, 1206 3 of 22

2. Geological Background

The ANS is a tract of juvenile continental crust formed during the Neoproterozoic era through the accretion of multiple island-arc terranes [17,18]. This process, driven by the closure of the ancient Mozambique Ocean, culminated in the collision of the East and West Gondwana continents, an event known as the East African Orogeny. The resulting orogenic belt is extensive, stretching from Saudi Arabia and Egypt southward through Northeast Africa [19].

Within the Eastern Desert and Sinai of Egypt, the exposed ANS basement complex is composed of five primary tectonostratigraphic units. These units, from oldest to youngest, are: (1) high-grade metamorphic gneisses and migmatites; (2) metasedimentary rocks derived from volcaniclastic arc material; (3) dismembered ophiolite sequences; (4) molasse-type sedimentary basins and Dokhan Volcanics; and (5) a suite of syn-, late-, and post-tectonic granitoid intrusions [18].

The granitoid rocks of the Egyptian ANS are broadly divided into two main age groups. The older group (750–610 Ma) consists of syn-tectonic, calc-alkaline I-type plutons (e.g., diorite, tonalite, trondhjemite, granodiorite). In contrast, the younger granitoids (610–580 Ma) were emplaced during late- to post-tectonic phases. These intrusions range from quartz monzonite to alkali granite and are characterized as either A-type or highly fractionated I-type granites [20].

The Wadi Al-Baroud area lies within the Northern Eastern Desert (NED) of Egypt, near its tectonic boundary with the Central Eastern Desert (CED) (Figure 1a). Neoproterozoic basement here comprises syn-tectonic tonalite–granodiorite, subordinate gabbro, and younger post-collisional biotite–muscovite monzogranite forming two plutons, Ras Baroud and Abu Hawis, which intruded the older granitoids along sharp contacts (Figure 1b). The older granitoids constitute the bulk of the exposure, show intense fracturing and exfoliation/spheroidal weathering, and contain abundant microgranular mafic enclaves; by contrast, the younger granites lack enclaves and truncate many dykes. The bedrock is dissected by faults and structurally controlled wadis, providing conduits for late-stage fluids and pegmatite emplacement [12,15].

Pegmatitic rocks in the area occur in two principal forms, plugs and dikes, emplaced inside the younger plutons and along their peripheries, and locally at the contacts with the older granitoids. Individual bodies are typically tabular to lensoid; widths range from several centimeters to several meters, with lengths from a few meters to several tens of meters. Dikes commonly exploit fracture zones and may extend from the interiors of the younger granites out into the older granitoids. Contacts are mostly sharp, though gradational margins occur where fluid saturation drove localized albitization and greisenization; narrow thermal aureoles are present where dikes/plugs cut the older granitoids. Miarolitic cavities are locally present, attesting to volatile-rich late-magmatic conditions [12,15].

Internally, pegmatites show simple but consistent zonation: a quartz–microcline core; an intermediate microcline–albite–muscovite zone (perthitic K-feldspar common); and an outer albite–muscovite rim. Accessory phases (zircon, monazite, xenotime, fluorite, and Nb–Ta-REEs oxides) are concentrated towards the outer zones. Two varieties are distinguished in hand specimen: pink K-feldspar-rich pegmatite (very coarse-grained) and white albite-rich pegmatite (medium-grained), both locally exhibiting graphic texture. Late albitization and muscovitization rims (and rare greisen selvages) are common along contacts and fractures, marking the magmatic–hydrothermal transition [12,15].

Radiometric measurements in the field show that most pegmatitic rocks are anomalously radioactive, with maxima where mica and iron-oxide aggregates are abundant. Natural-radioactivity indices from the southeastern Wadi Baroud sector (Abu Hadeida microgranitic offshoots) indicate very high gamma fields: mean absorbed

Minerals **2025**, 15, 1206 4 of 22

dose rate DR = 3929 ± 345 nGy h⁻¹ (n = 9), with AEDE_outdoor = 4.82 mSv y⁻¹ and AEDE_indoor = 19.3 mSv y⁻¹—values that exceed global averages by ~ $68\times$ (for DR and AEDE_outdoor) and ~ $48\times$ (for AEDE_indoor), respectively [21]. While these dose rates pertain to microgranitic dykes/veins within the Wadi Baroud system, unzoned pegmatitic plugs enclosed by younger granite at Gabal Abu Hawis can be internally non-radioactive, whereas contact-proximal pegmatites at the interface with older granitoids may be strongly radioactive [12].

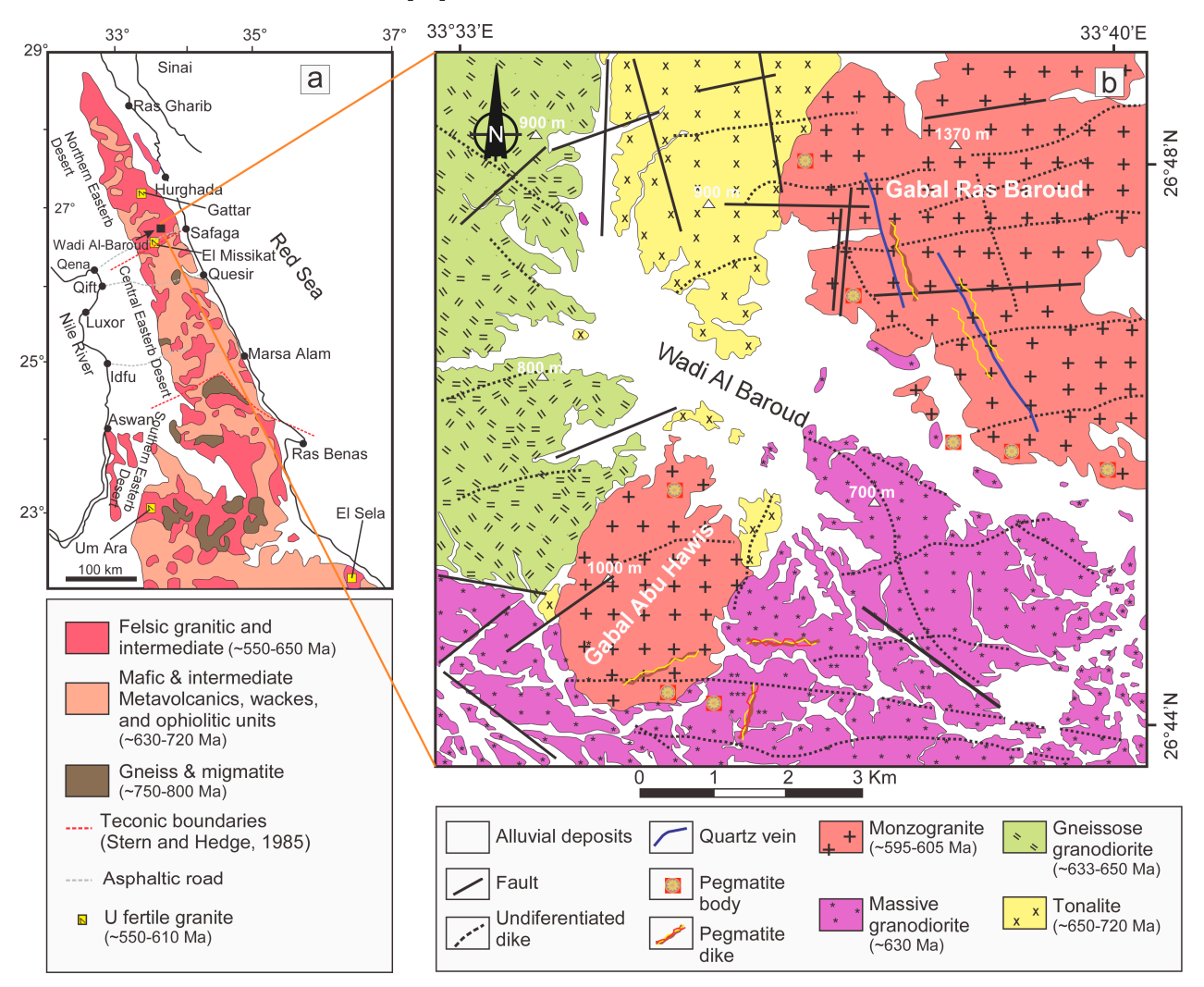


Figure 1. (a) Geological setting of the Eastern Desert of Egypt, with the study area at Wadi Al-Baroud indicated; (b) Local geology of the Wadi Al-Baroud area, highlighting the outcrop patterns of older and younger granitoids, as well as numerous pegmatite intrusions (Modified from Fawzy et al. [11]).

3. Analytical Methods

For the mineralogical investigation, polished thin sections were prepared and initially examined under an optical polarizing microscope at the Department of Lithospheric Research, University of Vienna (Austria). A representative suite of these samples was then selected for quantitative microanalysis. Following carbon coating, key minerals, including muscovite, columbite-(FeMnNb₂O₆), fergusonite-(YNbO₄), and euxenite-(Y,REE,U,Th)(Nb,Ta,Ti)₂O₈; from the rare-metal pegmatites and the host granites were analyzed using a CAMECA SX100 electron microprobe (EMP) at the Department of Lithospheric Research, University of Vienna, Austria. This instrument is equipped with wavelength-dispersive spectrometry (WDS) on spectrometers equipped with TAP, PET/LPET, and LIF/LLIF crystals. Primary standards were Y_ED (Y-Al-Si-Ca glass), Nb

Minerals **2025**, 15, 1206 5 of 22

metal ("nb"), REE glasses REE1/REE3/REE4, Nd_EDI, Sm_ED, Tm_ED, Yb_ED, Lu_ED, zircon (Zr), augite (AugitENM), thorianite, and UO2. X-ray lines, crystals, and standards were as follows: Si K α (TAP; zircon), Ti K α (PET/LPET; augite), Ca K α (PET/LPET; augite), Y L α (TAP; Y_ED), Nb L α (LPET; Nb metal), La L α (LLIF; REE3), Ce L α (LIF; REE3), Pr L β (LLIF; REE3), Nd L α (LLIF; Nd_EDI), Sm L β (LLIF; Sm_ED), Eu L α (LLIF; REE1), Gd L α (LLIF; REE1), Tb L α (LLIF; REE1), Dy L α (LLIF; REE4), Ho L β (LLIF; REE4), Er L β (LLIF; REE4), Tm L α (LLIF; Tm_ED), Yb L α (LLIF; Yb_ED), Lu M α (TAP; Lu_ED), Th M α (LPET; thorianite), and U M β (LPET; U2O3). For rare-earth elements, L-series lines (L α or L β , as specified above) were deliberately chosen to minimize interferences; off-peak backgrounds and matrix/interference (peak-overlap) corrections were applied throughout, with particular attention to critical REE overlaps.

Operating conditions were set to an accelerating voltage of 15 kV and a beam current of 20 nA, with a beam diameter of 1–5 μm depending on the mineral phase. For major elements, peak and background counting times were 20 and 10 s, respectively. Trace-element measurements employed longer counting times of 40–60 s on peaks and 20–30 s on backgrounds to enhance precision. The analytical procedure was calibrated using a combination of natural and synthetic standards. Raw data were corrected using the PAP matrix correction protocol.

4. Results and Discussion

4.1. Petrographic and Textural Features

The Wadi Al-Baroud rare-metal granite–pegmatite system exhibits pronounced coarse grain size and mineralogical variability, and a complex history of magmatic crystallization followed by intense late-stage hydrothermal overprinting (Figures 2 and 3).

Granite is medium- to coarse-grained, locally sheared at margins, and composed of quartz (34–42 vol%), K-feldspar (29–37 vol%), plagioclase (22–27 vol%), muscovite and biotite (2–5 vol%) and opaques (0.5–2 vol%) with rare amphibole (Figure 2a). Accessories include opaques, zircon, fluorite, monazite, and Nb-Ta oxides. Orthoclase (dominant) shows simple twinning and commonly contains plagioclase, quartz and muscovite inclusions. Microcline is subordinate and Fe-stained. Plagioclase exhibits albite twins with minor sericite. Quartz is interstitial/anhedral, embaying feldspars. Biotite in small anhedral flakes is partially altered to chlorite/opaques.

Pegmatites associated with the granites are coarse to very coarse grained and locally miarolitic, and they commonly show simple internal zonation with quartz-rich cores grading outward to feldspar- and mica-rich margins where accessory phases concentrate. They are composed of K-feldspar (20–50 vol%), albite (20–60 vol%), quartz (20–45 vol%), muscovite (3–10 vol%), biotite (0.5–5 vol%) and accessories (≤2 vol%; locally higher in pockets) (Figure 2b). K-feldspar occurs as orthoclase with perthitic lamellae and as microcline with tartan twinning. Albite forms euhedral prismatic to anhedral grains with polysynthetic (albite) twins, locally bent or broken, indicating post-magmatic strain. Quartz is generally anhedral with undulose extinction and may be included within feldspars and muscovite. Muscovite occurs as large subhedral to anhedral plates, while biotite is subordinate and commonly chloritized. Accessory phases comprise Nb-Ta-Y oxides, Fe-Ti oxides, zircon, monazite, xenotime, and fergusonite; they are not evenly distributed but preferentially accumulate in the feldspar-rich outer zones and along fractures, commonly with muscovite \pm Fe-oxides. Strategic Nb-Ta-Y-REE mineralization occurs in close association with these muscovite-iron oxide assemblages, reflecting strong geochemical partitioning of high-field-strength elements (HFSE) into the residual melt and late-stage fluids [13].

Minerals **2025**, 15, 1206 6 of 22

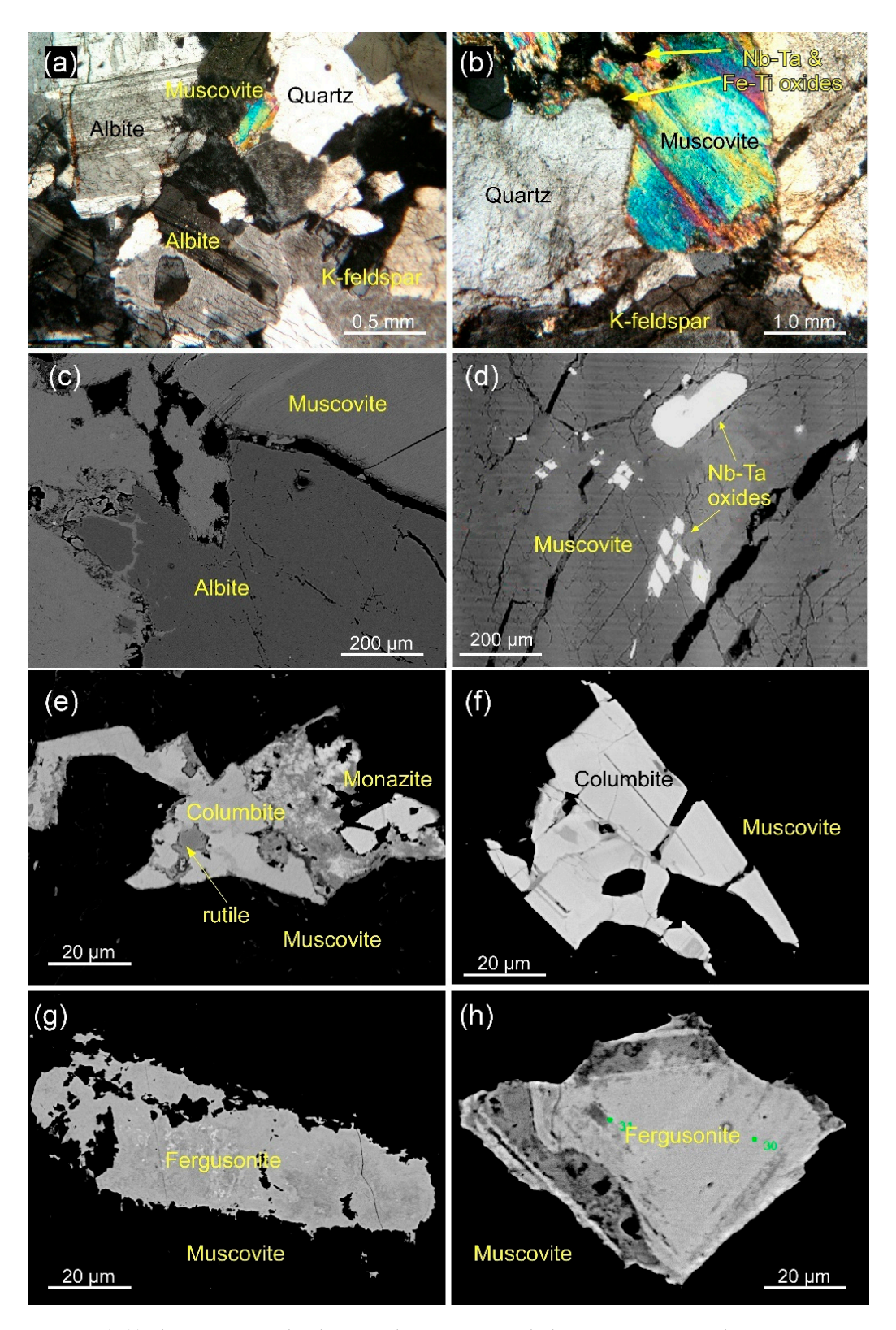


Figure 2. (a,b) Photomicrographs showing the main mineral phases in granites and pegmatites. Representative BSE images showing textures from the granite (c,e,g) and pegmatites (d,f,h). (c) Muscovite and albite intergrowth with micron-scale bright HFSE oxide inclusions along grain boundaries and fractures; (d) Muscovite hosting fracture-controlled Nb–Ta oxide pods aligned along fluid pathways; (e) Columbite with irregular embayed margins, rutile exsolution blebs, and monazite-(Ce) reaction rims recording fluid-induced re-equilibration; (f) Tabular columbite with straight edges and internal oscillatory zoning, indicating primary magmatic growth; (g) Fergusonite-(Y) occurring as elongate grains with mottled zoning and skeletal margins, reflecting partial replacement and chemical heterogeneity; (h) Fergusonite-(Y) with porous alteration rims and bright micron-scale inclusions, recording intense fluid-rock interaction and localized HREE enrichment.

Minerals **2025**, 15, 1206 7 of 22

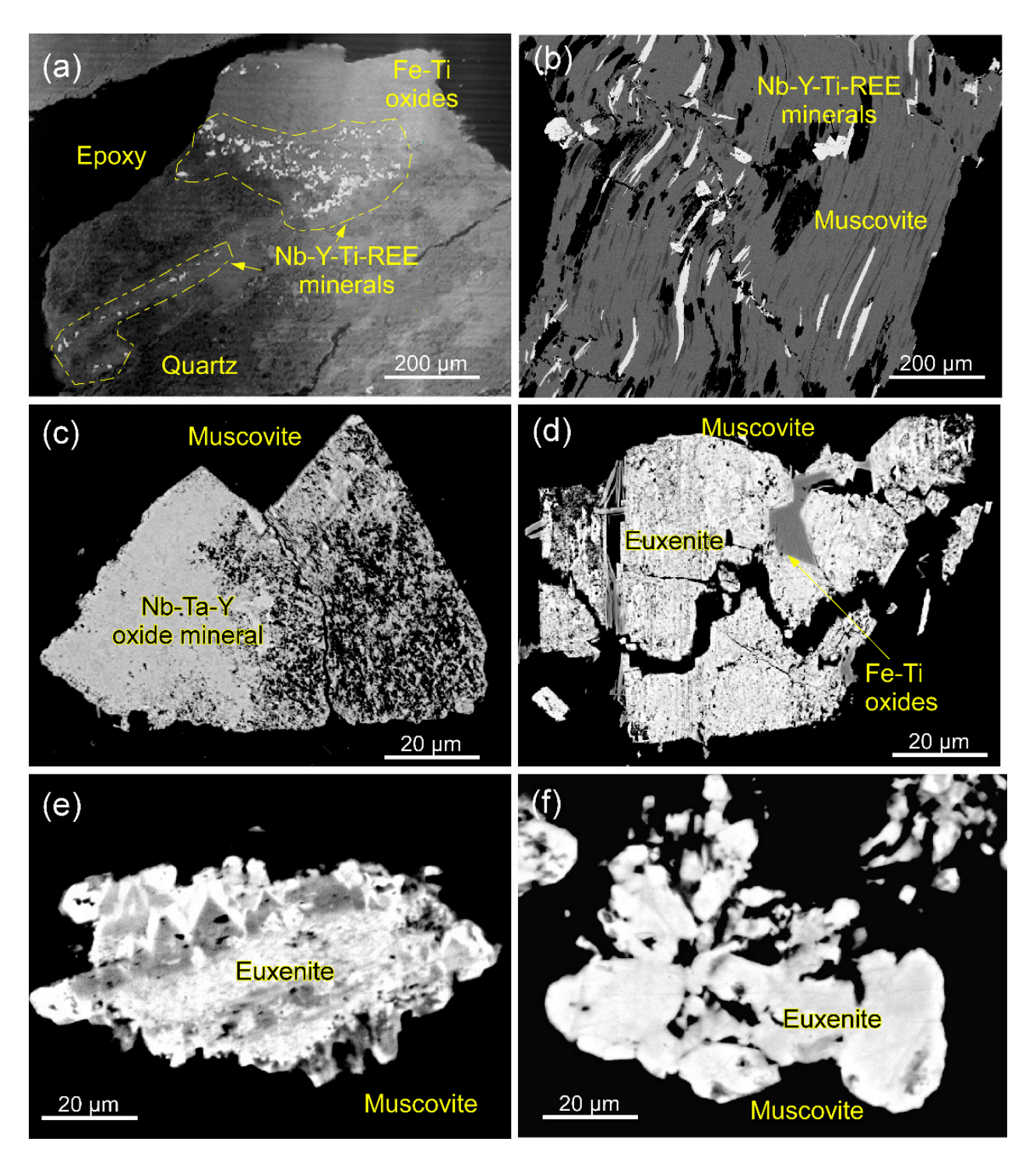


Figure 3. BSE images of accessory Y–Nb–Ti–REE oxides from pegmatitic domains. (**a,b**) Muscoviterich matrix hosting disseminated and fracture-controlled Nb–Y–Ti–REE oxides. (**c**) Y-rich Nb-Ta oxide mineral showing mottled zoning due to compositional changes during growth. (**d,e**) Euxenite-(Y) grains displaying highly fractured, porous textures formed by metamictization and fluid leaching. (**f**) Euxenite with irregular margins and patchy internal zoning, reflecting partial breakdown and redistribution by late-stage fluids. These features illustrate a complex evolution involving primary magmatic crystallization, structural control on HFSE mineral deposition, and significant hydrothermal overprinting.

Back-scattered electron (BSE) imaging reveals muscovite as the dominant matrix phase (Figure 2b), intergrown with albite and showing numerous inclusions and secondary alteration textures. Coarse muscovite plates truncate across a groundmass of fractured albite,

Minerals **2025**, 15, 1206 8 of 22

while micron-scale bright specks of Nb–Y–Ti oxides nucleate along mica–feldspar interfaces. This distribution indicates brittle deformation and fluid ingress concentrated along structural weaknesses, providing reactive pathways for HFSE mobilization and precipitation. In pegmatites, coarse muscovite aggregates are cut by open and healed fractures (Figure 2c), which host sharply bounded, equant Nb–Ta oxides. These oxides preferentially occur as pods or crack-fill phases aligned along fracture networks, demonstrating that late-magmatic or magmatic-hydrothermal fluids infiltrated these microstructures, precipitating columbite and related phases. The high BSE brightness of muscovite adjacent to these oxides suggests localized Fe–F enrichment.

Granite-hosted columbite (Figure 2d) occurs as irregular, embayed grains with pervasive internal fracturing and rutile exsolution blebs. The columbite rims are overgrown by monazite-(Ce), forming a distinct reaction halo that records late-stage fluid-rock interaction. The reaction sequence from columbite core \rightarrow rutile blebs \rightarrow monazite rim captures the progressive re-equilibration of Nb-oxide phases under fluid-rich conditions, involving Ti redistribution and precipitation of LREE–P phases at the interface [22]. These features attest to significant post-magmatic modification during hydrothermal overprint. Pegmatite-hosted columbite (Figure 2e) occurs as tabular crystals with straight edges. The lack of secondary reaction halos indicates minimal alteration and a predominantly magmatic origin. The brittle fragmentation of columbite along cleavage planes further suggests that late-stage deformation assisted in redistributing the HFSE-bearing melt, facilitating localized crystallization under extreme fractionation conditions [23].

Fergusonite-Y within granite (Figure 2f) occurs as elongate, massive grains characterized by mottled BSE zoning, irregular cracks, and skeletal margins. Such textures reflect intra-grain chemical heterogeneity (variations in Nb/Ta and Y/HREE ratios) and replacement of earlier Nb–Ti oxides during static fluid flow [24]. Fergusonite in pegmatites (Figure 2g) typically forms subhedral to euhedral crystals with concentric zoning and is surrounded by dark, porous reaction halos. These alteration halos, rich in micro-voids and secondary silicates, record intense F-rich fluid interaction and enhanced Y–HREE mobility.

Pegmatitic textures (Figure 3a,b) reveal abundant Nb–Y–Ti–REE oxides distributed within muscovite-rich domains and concentrated along micro-fractures and foliations. These oxides occur as disseminated inclusions, crack-fill textures, and replacement fronts, suggesting that structural focusing and late-stage fluid percolation played a decisive role in rare-metal concentration. Y-rich Nb-Ta oxides (Figure 3c) exhibit a distinct mottled BSE texture with alternating bright and dark sectors, indicative of subtle magmatic compositional fluctuations and oscillatory growth. Euxenite-Y (Figure 3d,e) occurs as fractured, porous grains with abundant voids and irregular crack networks. These brecciated textures are attributed to metamictization due to in situ U–Th decay, followed by fluid-induced leaching and partial chemical redistribution. Euxenite (Figure 3f) displays irregular margins, patchy zoning, and pervasive internal corrosion, features characteristic of metamict breakdown and fluid-mediated alteration. These secondary textures attest to a complex post-magmatic history involving structural damage, leaching, and re-precipitation of HFSE phases under fluid-rich conditions.

Taken together, the textural and mineralogical observations reveal a multistage paragenetic sequence in the Wadi Al-Baroud granite–pegmatite system, beginning with the primary magmatic crystallization of quartz, feldspar, and muscovite, accompanied by the early formation of Nb–Ta oxides such as columbite and fergusonite. Subsequent structural focusing and fracture development created permeable pathways that allowed residual melts and fluids to infiltrate the system and precipitate additional HFSE-bearing minerals. This was followed by extensive hydrothermal reworking and metamictization, resulting in the formation of reaction rims, rutile exsolution textures, monazite halos, and porous alteration

Minerals **2025**, 15, 1206 9 of 22

fabrics, particularly within U/Th-rich phases like euxenite. Late-stage F-rich fluid circulation further facilitated the localized enrichment and redistribution of Y, HREE, and LREE, overprinting earlier mineral assemblages. Collectively, these processes demonstrate that rare-metal mineralization was driven by the interplay of magmatic fractionation, tectonic deformation, and hydrothermal re-equilibration, with muscovite serving both as a primary rock-forming phase and a secondary repository for HFSE during post-magmatic alteration. The close spatial and structural association of Nb–Ta–Y–REE oxides with muscovite and fracture networks highlights the pivotal role of fluid–rock interaction in concentrating strategic metals during the final stages of pegmatite evolution.

4.2. Composition and Crystal-Chemical Evolution of Muscovite: Substitution Mechanisms and Fluorine Enrichment

The chemical composition of muscovite from the Wadi Al-Baroud granite–pegmatite system (Table S1) reveals clear distinctions between the granite- and pegmatite-hosted micas, reflecting different crystallization conditions, volatile contents, and post-magmatic histories. The low totals reflect the presence of volatile components (OH, H₂O) and possibly light elements (Li, B). Pegmatitic muscovite is consistently enriched in SiO₂ (up to ~46.7 wt.%), FeO (5.3–7.8 wt.%), MgO, MnO, K₂O, and especially fluorine (2.2–4.34 wt.%), whereas granitic muscovite shows slightly lower SiO₂ (~46 wt.%), lower FeO (~5.3–5.5 wt.%), and significantly reduced F contents (~1.8–2.0 wt.%). Structurally, pegmatitic muscovite contains higher interlayer K (up to ~1.95 apfu) and enhanced octahedral Fe²⁺ and Mg (up to ~0.91 and ~0.45 apfu, respectively), while granite-hosted muscovite retains higher octahedral Al (4.70–4.96 apfu). These compositional contrasts reflect crystallization from a more evolved, volatile-rich melt in the pegmatites and a relatively early, less differentiated stage in the granites.

On the Mg–Na–Ti ternary diagram (Figure 4a, [22]), muscovite compositions from both rock types plot across the boundary between primary and secondary muscovite fields, indicating a multistage evolution. Granite muscovites cluster tightly within the primary field, suggesting crystallization directly from the melt, whereas pegmatitic muscovites display a broader spread and elevated Ti contents, reflecting late-stage melt evolution and possible fluid–rock interaction. The substitution trends observed in these micas further support this interpretation. The strong positive correlation between tetrahedral Si and octahedral cations (Mg + Fe) (Figure 4b) demonstrates the dominance of Tschermak–phengitic substitution ([Fe²⁺, Mg] + Si⁴⁺ \rightarrow Al^{IV} + Al^{IVI}) [22], with pegmatitic muscovite plotting at the high-Si, low-Al end of this trend (Figure 4c). This shift reflects enhanced celadonitic (phengitic) substitution, associated with advanced magmatic differentiation and higher volatile activity [25]. This is supported by the (Fe + Mg)/(Fe + Mg + Ti + Al) vs. Na/(Na + K + Ca) plot (Figure 4d), which points to a strong celadonite component and confirms crystallization from highly fractionated, Fe–Mg–Si-rich melts.

A partial decoupling of Fe from the Si–Mg substitution trend (Figure 4e) points to the operation of ferrimuscovite substitution (Fe³+ \leftrightarrow Al IVI) under slightly oxidizing or F-rich conditions, a feature more pronounced in pegmatite than granite muscovite. Finally, paragonitic substitution (K+ \leftrightarrow Na+) is evident in both rock types (Figure 4f), though pegmatitic muscovite shows slightly higher K and Na contents and occasional site vacancies, suggesting the incorporation of alkalis (Na, Rb, Cs) during crystallization and later hydrothermal alteration. These geochemical trends and substitution mechanisms demonstrate that muscovite in the Wadi Al-Baroud system records a complex history involving primary magmatic crystallization, strong volatile influence, and late-stage fluid modification.

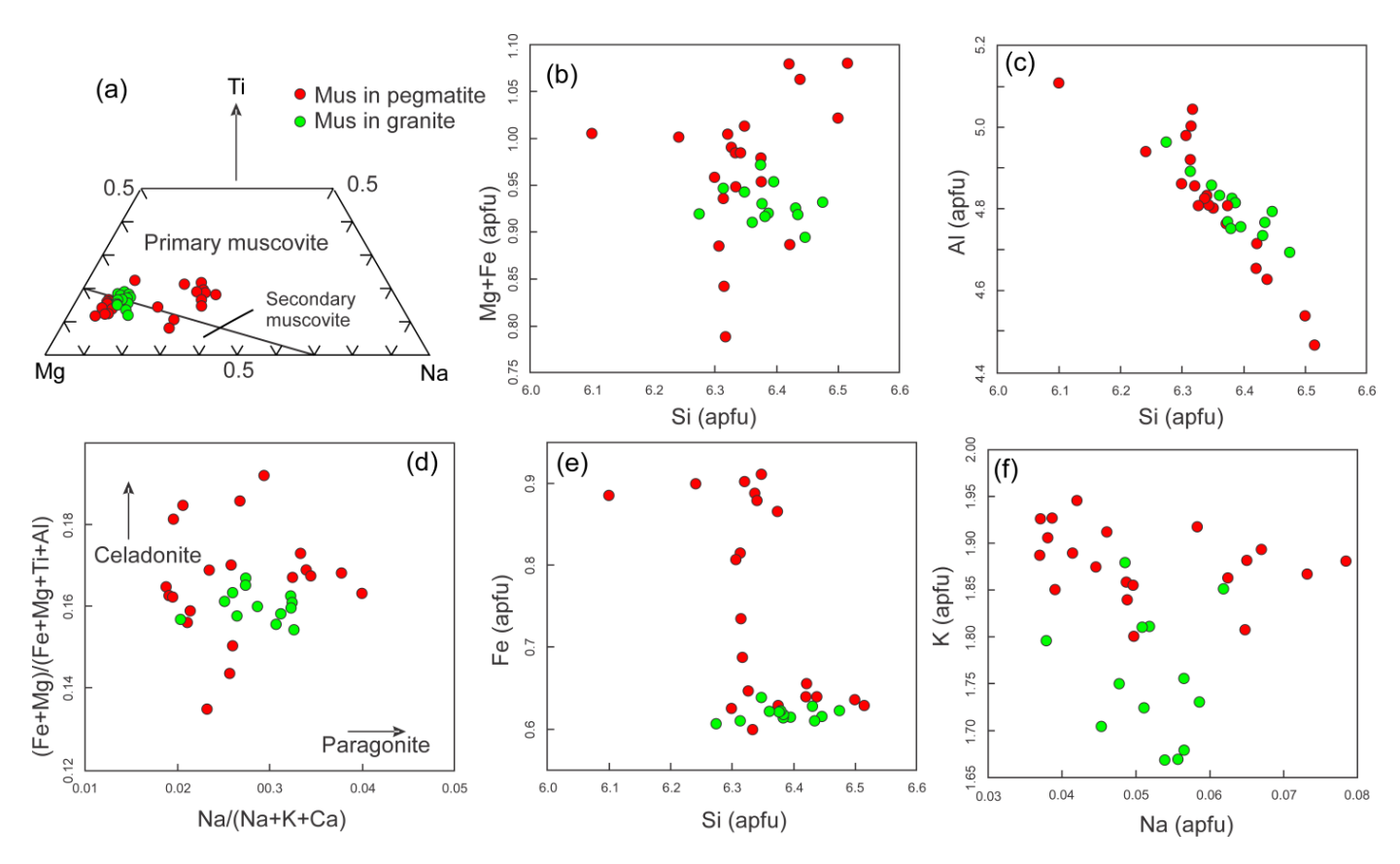


Figure 4. (a) Ternary Mg–Ti–Na diagram for muscovite of the Wadi Al-Baroud area, Eastern Desert of Egypt, discriminating between primary and secondary muscovite (after Miller et al. [22]); (b) Chemical composition diagram of the muscovite from Wadi Al-Baroud rare metal pegmatite and granite, Eastern Desert of Egypt (after Clarke [26]); (c) Si vs. Mg+Fe diagram; (d) Si vs. Al diagram; (e) Si vs. Fe diagram; (f) Na vs. K diagram.

Fluorine plays a critically important role in driving this chemical evolution. Because F is incompatible in feldspar and quartz, it concentrates in the residual melt and partitions strongly into late-crystallizing micas and coexisting fluids [27]. The elevated fluorine contents in pegmatitic muscovite (up to 4.34 wt.%) indicate crystallization from an F-saturated melt, where fluorine complexing was significant. High F concentrations lower the melt viscosity and solidus temperature, prolonging crystallization and enhancing the solubility and transport of HFSE and rare elements. In the Wadi Al-Baroud system, F-rich conditions likely stabilized the Si-rich muscovite structure, promoted extensive celadonitic substitution, and facilitated extreme HFSE fractionation. Notably, however, fluorine enrichment is not directly coupled with iron enrichment. This decoupling suggests that F incorporation depends more on the availability of Al–OH sites and fluid composition, whereas Fe uptake reflects redox evolution and melt chemistry [28]. As a result, fluorine acted primarily as a fluxing agent, enhancing melt mobility and element transport, while iron enrichment records oxidation-state changes and compositional evolution of the host system [29].

4.3. Fractionation Trends in CGMs

The geochemical composition of CGMs from the Wadi Al-Baroud granite–pegmatite system provides critical insights into the magmatic evolution and fractionation history of the host rocks. Electron microprobe analyses (Table S2) reveal pronounced compositional contrasts between granite-hosted and pegmatite-hosted columbite, reflecting distinct crystallization environments and degrees of magmatic differentiation. Granite-hosted

columbite-(Fe) is Nb-rich and Mn-dominant, with Nb₂O₅ contents of ~71–76 wt.% and Ta₂O₅ of only 1.3–6.0 wt.%, yielding low Ta/(Ta + Nb) ratios of 0.01–0.05. In contrast, pegmatite-hosted columbite is significantly more evolved, characterized by reduced Nb₂O₅ (~55–58 wt.%) and enriched Ta₂O₅ (~14.6–16.7 wt.%), corresponding to Ta/(Ta + Nb) ratios of 0.13–0.15. Manganese content also varies considerably, with granite CGMs containing MnO = 14.27–14.79 wt.% compared to 10.67–12.32 wt.% in pegmatitic CGMs. HREEs enrichment is more pronounced in the pegmatite columbite, with Dy₂O₃ ranging from 2.3–3.3 wt.% compared to 0.6–1.6 wt.% in granite equivalents. These compositional signatures collectively indicate that pegmatite-forming melts were more strongly fractionated and enriched in Ta, Mn, and HREEs compared to the granitic precursors, recording a progressive magmatic evolution toward more specialized, rare-metal-rich conditions.

The chemical data also reveal that CGMs from Wadi Al-Baroud pegmatites are significantly more evolved, with lower Mn/(Mn + Fe) and higher Ta/(Ta + Nb) ratios compared to their granitic counterparts (Figure 5a). Most samples plot within the columbite-(Mn) field, with pegmatitic compositions extending toward the columbite-(Mn)–columbite-(Fe) boundary. While the data diverge from the field defined by CGMs from Graciosa, Brazil [30], they show clear compositional overlap with those from the Totoral pegmatite, Argentina [31]. Moreover, they closely align with published data from the Ras Baroud granite–pegmatite system, including subsets with extremely high Ta/(Ta + Nb) ratios.

Further insights into the evolutionary paths of CGMs are evident from the Nb/Ta vs. Mn/Fe plot (Figure 5b). Granite-hosted CGMs define a nearly horizontal trend, with a broad Nb/Ta range (19.5–100) and consistently high Mn/Fe ratios (1.82–2.13), characteristic of manganocolumbite crystallization from a less-evolved, higher-temperature melt where Fe^{2+} availability was limited by early silicate crystallization (e.g., biotite, amphibole) [32,33]. In contrast, pegmatite-hosted CGMs define a vertical array with low Nb/Ta (5.56–6.57) and low Mn/Fe (0.88–1.07), plotting near the manganocolumbite–manganotantalite boundary. This pattern reflects crystallization from a highly fractionated, F- and H₂O-rich melt where Ta enrichment preceded CGM saturation [34,35], and Mn depletion was likely linked to early garnet crystallization. The limited Mn/Fe variation suggests that local redox conditions or fluid–melt partitioning, rather than major Nb–Ta fractionation, controlled the observed trend [36].

Y-rich Nb-Ta mineral compositions provide additional evidence for melt heterogeneity and the timing of crystallization events. As shown in the inset of Figure 5b, Y-rich Nb-Ta grains from the pegmatite display high Nb/Ta ratios (\sim 5.22–6.78) and low Mn/(Mn + Fe) (\sim 0.69), defining a distinct negative correlation that diverges from the main pegmatitic columbite trend [37]. This geochemical signature indicates crystallization from a less evolved, Nb-rich melt pocket that had concentrated Y and Ti but had not yet undergone significant Ta enrichment or Mn incorporation [38]. Comparable signatures are observed in early-stage CGMs from other rare-element pegmatites, such as the Little Nahanni pegmatites in Canada [39], highlighting the presence of internal melt heterogeneity crystallization in the Wadi Al-Baroud system.

The relationship between Ta enrichment and HREEs incorporation is shown in Figure 5c, where Ta/(Ta + Nb) exhibits a strong positive correlation with Dy content. Granite CGMs with low Ta/(Ta + Nb) (\leq 0.05) incorporate minimal Dy, whereas pegmatitic CGMs with higher Ta/(Ta + Nb) (\approx 0.14–0.15) host significantly more Dy, indicating that HREE incorporation occurs predominantly in highly evolved, residual melts. The systematic Nb–Ta anti-correlation (Figure 5d) further illustrates this progressive fractionation, where granite CGMs start as Nb-rich (\sim 1.9 apfu Nb, \sim 0.05 apfu Ta) and evolve toward Ta-rich compositions (\sim 1.59 apfu Nb, \sim 0.27 apfu Ta), consistent with fractionation trends reported from Ras Baroud pegmatites and the Preissac–Lacorne system in Que-

bec [40]. Y-rich Nb-Ta mineral compositions, with intermediate Nb (~0.67–0.69 apfu) and low Ta (~0.05–0.07 apfu), capture an intermediate stage of Nb depletion and incipient Ta enrichment prior to complete Ta saturation.

Additional compositional differences between granite- and pegmatite-hosted CGMs are illustrated in Figure 5e. Granite columbite shows a tightly clustered, Mn-rich/Fe-poor composition (FeO = 5.43–6.23 wt.%), whereas pegmatite columbite displays a ferroan trend with higher FeO (8.37–9.69 wt.%) and lower MnO (10.67–12.32 wt.%), reflecting a solid-solution series between manganocolumbite and ferrocolumbite [41]. This trend records magmatic fractionation processes during pegmatite evolution. Y-rich Nb-Ta minerals compositions are scattered due to significant Y and Ti incorporation, where Y³⁺ + REE³⁺ substitution into the A-site, charge-balanced by vacancies or Ti⁴⁺, reduces the structural requirement for Fe/Mn in the B-site [42].

The role of volatiles in HFSE mobility and late-stage enrichment is highlighted by positive correlations between Ta/(Ta + Nb) and Ti contents in pegmatitic columbite (Figure 5f). These trends suggest that complexing ligands such as F^- and $PO_4{}^{3-}$ maintained Ti solubility in the residual melt until late stages [43]. Y-rich Nb-Ta mineral, crystallizing earlier, contains intermediate Ti (~0.51–0.55 apfu), whereas pegmatitic columbite reaches higher Ti contents (~0.60 apfu), reflecting late crystallization under F-rich conditions.

The data conclude that the compositional evolution of CGMs from Wadi Al-Baroud records a clear progression from an Nb–Fe–dominant, Mn-rich assemblage in granite to a Ta–Fe–Mn–HREE-enriched assemblage in pegmatite, with Y-rich phases representing an intermediate evolutionary stage. This transition was driven by advanced magmatic fractionation, volatile-rich conditions, and late-stage hydrothermal reworking, collectively producing the characteristic Nb \rightarrow Ta and Fe \rightarrow Mn shifts observed in highly evolved rare-metal pegmatite systems.

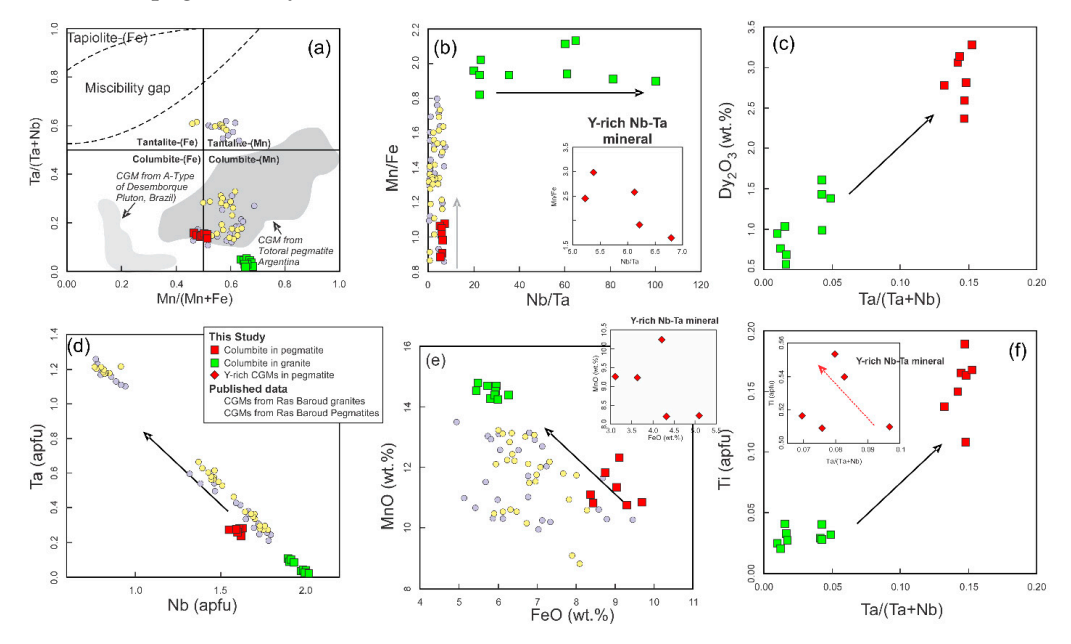


Figure 5. (a) Chemical composition of the columbite from Wadi Al-Baroud rare metal pegmatite and granite, Eastern Desert of Egypt, plotted in the Mn/(Mn + Fe) vs. Ta/(Ta + Nb) columbite-tantalite quadrilateral classification diagram. The miscibility gap is according to Černý et al. [41]. Comparison data of columbite from reduced A-Type granites of Desemborque Pluton, Brazil, were obtained from Siachoque et al. [30]. Comparison data of Nb-Ta oxides from Totoral LCT rare-element pegmatite district, San Luis, Argentina were obtained from Galliski et al. [44]; (b) Nb/Ta vs. Mn/Fe diagram; (c) Ta/(Ta + Nb) vs. Dy₂O₃ diagram; (e) Nb vs. Ta; (d) Nb vs. Ta; (e) FeO vs. MnO; (f) Ta/(Ta + Nb) vs. Ti diagrams. Comparison data of CGMs from Ras Baroud granites and pegmatites after Abuamarah et al. [15] and Matta et al. [45], respectively.

4.4. Compositions and Crystal-Chemical Evolution of Y-Nb-Ti Oxides

The Y-Nb-Ti oxides at Wadi Al-Baroud (fergusonite-Y, euxenite-Y), together with Y-rich Nb-Ta phase discussed previously, crystallized during the late stages of melt evolution and collectively record the interplay among extreme fractionation, F-rich fluids, and subsequent alteration. Fergusonite-Y occurs in both granite and pegmatite, whereas euxenite-Y is confined to pegmatitic pods (Figure 3). Pegmatite-derived fergusonite is systematically enriched in high-field-strength and other incompatible elements relative to granite fergusonite (Table S4), containing $Ta_2O_5 = 0.9-5.4$ wt.%, $UO_2 = 1.2-2.0$ wt.%, and ThO₂ = 2.5-4.1 wt.%, compared with $\sim 0.9-1.1$ wt.% Ta₂O₅, 0.06-0.14 wt.% UO₂, and 0.2–0.3 wt.% ThO₂ in the granite counterpart. In parallel, granite fergusonite shows lower TiO₂ (1.4–3.6 wt.%) but higher FeO (0.7–2.1 wt.%), whereas pegmatitic fergusonite exhibits higher TiO₂ (2.5–4.7 wt.%) but distinctly lower FeO (0.2–0.4 wt.%). We interpret the higher TiO₂ yet much lower FeO in pegmatitic fergusonite as the signature of a highly fractionated, Fe-depleted residual melt, comparatively rich in Ti and incompatible species, from which fergusonite crystallized late under more oxidized conditions. By contrast, earlier crystallization in the granite from a less fractionated, Fe-richer melt allowed greater Fe substitution in fergusonite; subsequent pegmatitic hydrothermal alteration may have further stripped Fe from fergusonite [46]. This scenario accords with general models of REE-Ti-oxide mineralization in specialized pegmatites, wherein extreme fractionation and volatile-mediated complexing concentrate HFSE and REE in late accessory phases.

Recalculated formulae emphasize these differences, where pegmatite fergusonite averages ~0.03–0.05 apfu Th and 0.01–0.02 apfu U, compared to ~0.001–0.003 Th and ~0.0005 U in granite fergusonite; pegmatitic crystals also host slightly more Ta (~0.02–0.07 apfu vs. ~0.01). Conversely, granite fergusonite is poorer in Ti (0.05–0.11 apfu vs. ~0.10–0.15 in pegmatite) but richer in Fe (0.02–0.08 apfu vs. 0.02–0.05 in pegmatite). This compositional inversion (i.e., lower Ti, higher Fe in granite fergusonite versus higher Ti, lower Fe together with strong Ta–U–Th enrichment in pegmatitic fergusonite), records progressive magmatic fractionation. The less-evolved granitic melts accommodated more Fe in fergusonite, while extreme fractionation and volatile-rich residual melts in the pegmatitic stage concentrated Ti and incompatible HFSE/actinides (Ta, U, Th, Y/HREE), subsequently incorporated into late fergusonite; redox evolution and late hydrothermal modification likely amplified Fe depletion and actinide uptake in pegmatite-hosted grains [47].

Euxenite-Y captures an even more evolved snapshot of the residual pegmatitic chemistry. Its restriction to pegmatite implies that only the pegmatitic regime attained the requisite combination of high Y + REE, Nb + Ta, Ti, and volatile activity to stabilize these complex oxides. Both minerals approximate (Y, REE, U, Th)₂(Nb, Ta, Ti)₂O₈ and display exceptional concentrations of incompatible elements. Euxenite-Y contains ~23.5–32.8 wt.% Nb_2O_5 and 11.1–14.5 wt.% Ta_2O_5 . It is rich in TiO_2 (18–21 wt.%) and Y_2O_3 (~17–20 wt.%). Its chondrite-normalized REE patterns (Figure 6a) show steep LREE depletion (La-Sm) and elevated, comparatively flat HREE segments through Lu. These signatures indicate an LREE-poor parental melt, whether by early monazite/allanite crystallization or source inheritance, further modified by F-complexation that kept Y and HREE mobile until late oxide saturation. Because F⁻ forms stable complexes with smaller, higher-charge cations (HREE³⁺, Y³⁺, Nb⁵⁺, Ta⁵⁺), REE are effectively fractionated, where HREE remain mobile, whereas LREE are depleted or earlier sequestered [48]. At Wadi Al-Baroud, elevated Y/Dy ratios quantify this effect, ~12–23 in euxenite-Y, implying preferential F-complexation of Dy (and other HREE) that leaves Y in relative excess by the time of oxide crystallization [48]. In lower-F pegmatites (e.g., Julianna, Poland [49]), analogous minerals show much lower Y/Dy, underscoring the intensely F-rich conditions of Wadi Al Baroud.

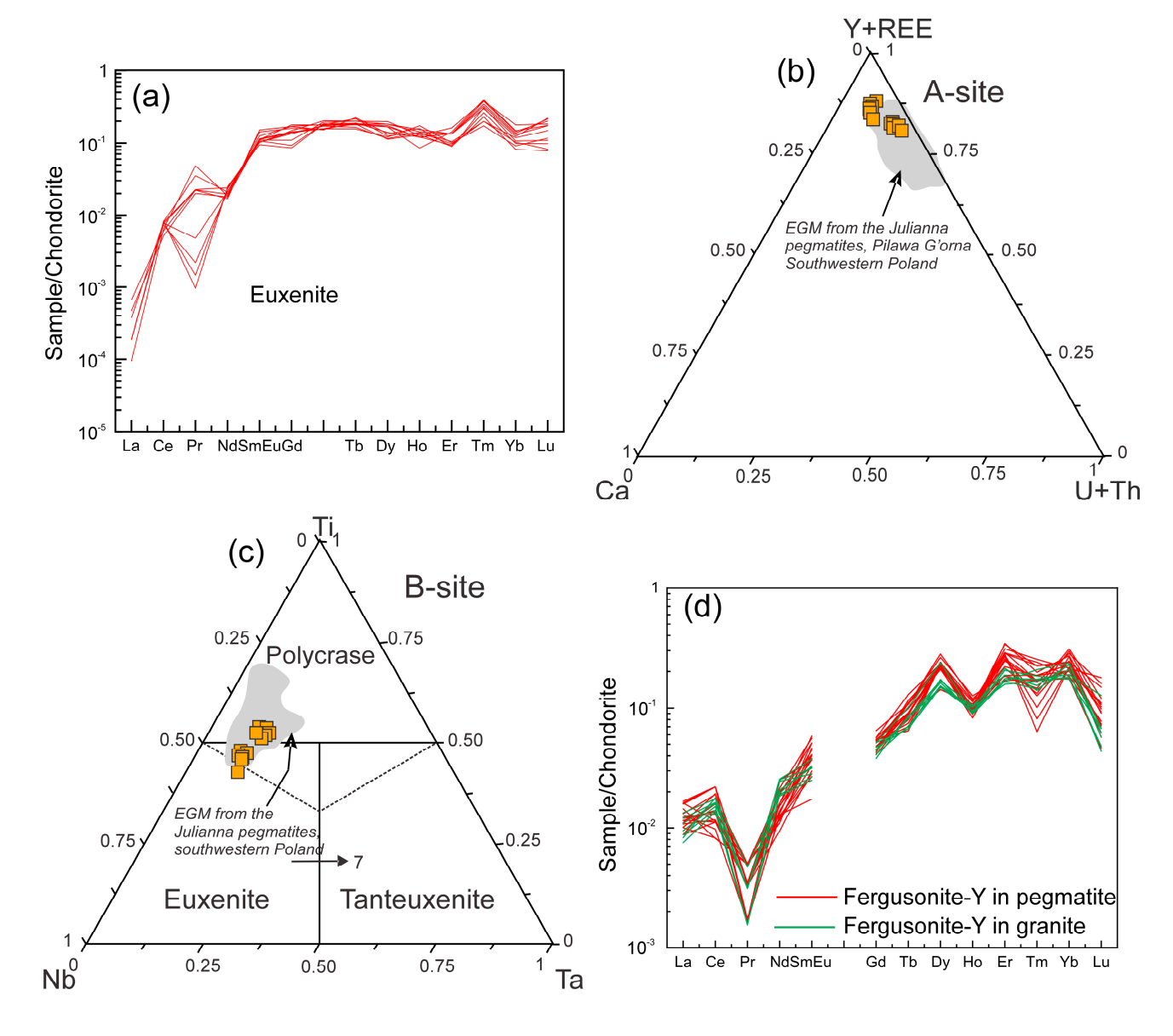


Figure 6. (a) Chondrite-normalized rare earth element (REE) patterns for euxenite-(Y); (b,c) Ternary diagrams illustrating A-site (Y+REE–Ca–U+Th) and B-site (Ti–Nb–Ta) cation occupancies for euxenite-group minerals from both pegmatite and granite samples. Compositional fields are delineated according to the dominant-valency rule [50] (solid lines) and the assumption of Ti, Nb, and Ta as equivalent components [49] (dotted lines). Data from the Julianna pegmatite, Poland [49] are included for comparison; (d) Chondrite-normalized rare earth element (REE) patterns for fergusonite-(Y) minerals in pegmatites and granites from Wadi Al-Baroud area, Eastern Desert of Egypt.

Euxenite-Y contains \sim 3.6–8.6 wt.% UO₂ and 0.5–2.8 wt.% ThO₂. This elevated U–Th likely accounts for extensive metamictization (patchy zoning, pervasive fracturing) seen in Figure 3e,f). In euxenite, the A-site is dominated by Y + REE (total \sim 0.76–0.82 apfu; Y \sim 0.6; REE \sim 0.16–0.22), and Nb > Ta at the B-site (Ti/(Ti + Nb + Ta), generally 0.45–0.54. By modern classification criteria and compositional plots (Figure 6b,c), the Wadi Al-Baroud analyses fall squarely within euxenite-Y fields, matching those from other highly fractionated pegmatites (e.g., Polish Sudetes [49]).

Fergusonite-(Y) is noteworthy for concentrating Y, REE, U, and Th in both granite and pegmatite. Its REE patterns (Figure 6d) are strongly fractionated, with very low LREE (LaNd), deep troughs at Pr–Nd, and convex-upward HREE segments peaking at Dy–Er–Yb, accompanied by diagnostic negative Tm and Lu anomalies, crystal-chemical expressions of

Minerals **2025**, 15, 1206 15 of 22

size-selective site occupation (Tm³⁺ and Lu³⁺, with very small ionic radii, are less easily accommodated than slightly larger HREE or Y³⁺). Strong LREE depletion is consistent with early LREE scavenging by monazite-(Ce)/allanite-(Ce), leaving the melt progressively enriched in HREE + Y [51]. Pegmatite fergusonite typically achieves the highest Σ REE, Y, U, and Th of any oxide in the system, reflecting crystallization from a more evolved, REE-rich fluid [52].

Compositional systematics sharpen the granite–pegmatite variation. In Y/(Nb + Ta) vs. Σ REE space (Figure 7a), granite fergusonite forms a tight cluster at lower Σ REE (0.15–0.17 apfu) and higher Y/(Nb + Ta) (0.54–0.58), whereas pegmatite fergusonite spans higher Σ REE (0.17–0.21 apfu) and lower Y/(Nb + Ta) (0.49–0.54), with some grains extending to higher Y/(Nb + Ta) at similar Σ REE. This divergence indicates decoupled Y–REE incorporation in the two hosts: early, less-fractionated granitic melts favored Y uptake relative to Nb+Ta (and lower total REE), while late pegmatitic melts—subject to advanced fractionation and enhanced fluid–melt interaction—promoted substantially higher REE incorporation at modest Y/(Nb + Ta) [53]. The decrease in Y/(Nb + Ta) with increasing Σ REE in pegmatitic fergusonite points to competitive substitution between Y and light-to-middle REE for analogous crystallographic sites, a behavior reported in other rare-metal pegmatite provinces [54].

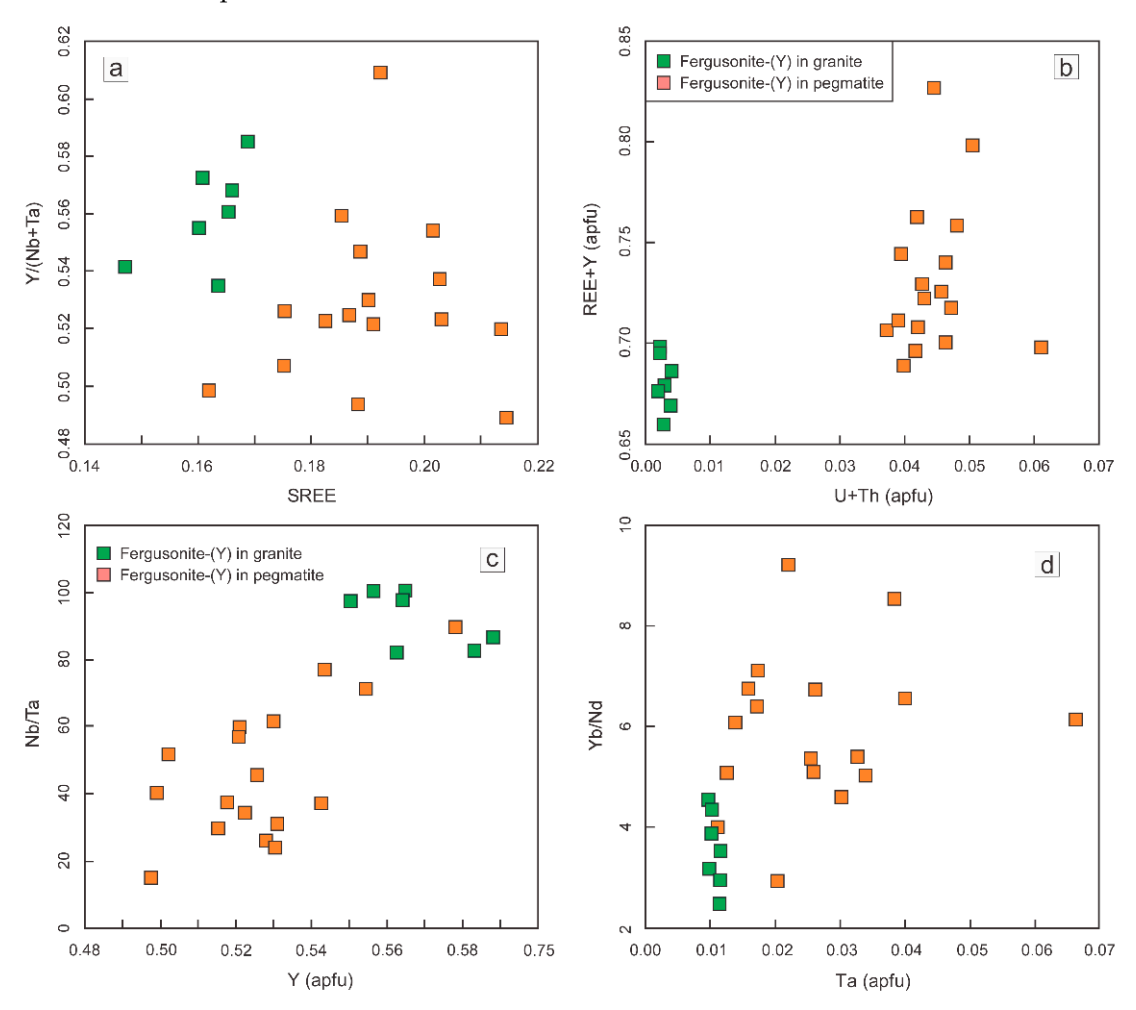


Figure 7. Compositional variation of fergusonite-(Y) from granite and pegmatite illustrating progressive magmatic fractionation trends: (a) Σ REE vs. Y/(Nb + Ta) showing higher Σ REE contents and lower Y/(Nb + Ta) ratios in pegmatitic fergusonite; (b) Positive correlation between (U + Th) and (Σ REE + Y) indicating co-enrichment of incompatible elements in pegmatitic samples relative to granitic ones; (c) Negative correlation between Y and Nb/Ta; (d) Positive correlation between Ta and Yb/Nd.

A strong positive correlation between (U+Th) and (Σ REE+Y) (Figure 7b) further attests to co-enrichment of actinides and REE + Y in the pegmatitic stage, far exceeding granite levels, mirroring a residual fluid that, by solidification, had accumulated very high concentrations of U-Th together with REE + Y. The Y versus Nb/Ta relation (Figure 7c) reveals a clear petrogenetic divergence, where granite fergusonite shows higher Y (0.55–0.59 apfu) paired with elevated Nb/Ta (82.1–101), consistent with earlier crystallization from a less-evolved melt where Y entered fergusonite readily and Nb dominated over Ta [55]. Pegmatite fergusonite plots at lower Nb/Ta (14.78–89.70) and generally lower Y (0.50–0.58 apfu), signaling extensive fractionation and progressive Ta enrichment in the residual melt. Finally, Y vs. Yb/Nd (Figure 7d) shows a positive correlation distinguishing pegmatite (high Yb/Nd, high Y, but scattering due to local heterogeneity) from granite (lower, tighter cluster), tracking the progressive HREE \gg LREE bias in the terminal pegmatitic rocks [56].

These mineral chemistry data demonstrate a coherent evolutionary pathway, where early granite fergusonite fixes Ti (\pm Nb, Y) from comparatively hotter, less volatile melts, while late pegmatitic fergusonite and euxenite-Y crystallize from F-rich, highly fractionated residual liquids that concentrate Ta, U, Th, Y, and HREE. Volatile complexing, redox evolution, and localized hydrothermal overprinting together governed the final distribution of strategic elements in this highly evolved rare-metal pegmatite system. For clarity, the principal granite–pegmatite contrasts and crystal-chemical mechanisms are synthesized in Table 1.

Table 1. Comparative crystal-chemical mechanisms in Y–Nb–Ti oxides from granite vs. pegmatite at Wadi Al-Baroud.

Indicator/Mechanism	Granite (Fergusonite-(Y))	Pegmatite (Fergusonite-(Y), Euxenite-(Y))	Interpretation
TiO ₂ (wt.%)	1.4–3.6	2.5–4.7 (Ferg-Y); 18–21 (Eux-Y)	Ti enrichment with advanced fractionation/pegmatitic stage
FeO (wt.%)	0.7–2.1	0.2–0.4 (Ferg-Y)	Fe depletion in late, more oxidized, volatile-rich melts
Ta ₂ O ₅ (wt.%)	~0.9–1.1	0.9–5.4 (Ferg-Y); 11.1–14.5 (Eux-Y)	Progressive Ta enrichment during fractionation
UO ₂ + ThO ₂ (wt.%)	≤0.5	up to ~8.6 UO ₂ ; 0.5–2.8 ThO ₂ (Eux-Y)	Late actinide uptake, metamictization tendency
Y/(Nb + Ta)	0.54-0.58	0.49–0.54 (broader tail)	Decoupling of Y vs. REE in pegmatite
ΣREE (apfu, Ferg-Y)	0.15-0.17	0.17–0.21	Higher total REE in pegmatite
Nb/Ta (molar)	82–101	14.8–89.7	Ta-ward evolution in pegmatite
Y/Dy (Eux-Y)	_	~12–23	F-rich conditions; HREE mobility vs. Y excess
REE patterns	LREE-poor, moderate HREE	Strong LREE depletion; HREE-Y rich	F-complexation and late oxide saturation

Minerals **2025**, 15, 1206 17 of 22

4.5. Petrogenetic Controls on Rare-Metal Enrichment

The mineralogical and geochemical attributes of the Wadi Al-Baroud system indicate a rare-metal enrichment pathway governed by volatile-rich magmatic differentiation working in tandem with structural controls that localized deposition. By the final stages of crystallization, the pegmatitic melt was saturated in volatiles—chiefly H₂O and F, which exerted first-order control on partitioning behavior. Fluorine acted as a powerful flux, where it lowered melt viscosity and solidus temperature, extended the crystallization interval, and promoted extreme fractionation of HFSE and REE via the formation of stable complexes [57]. Mineral chemistry supports this assumption where pegmatitic muscovite is F-rich (to ~4 wt.%) and Si-enriched, consistent with growth from a highly differentiated, F-bearing fluid, while the high Y/Dy ratios and HREE-rich signatures in euxenite point to strong F-REE complexation in the melt. These volatiles enhanced the solubility and transport of Ta, Nb, Y, and HREE, suppressing premature crystallization and allowing progressive buildup in the residual liquid [58]. Consequently, late phases such as pegmatitic columbite and fergusonite-Y precipitated with unusually high loads of incompatible elements (Ta, U, Th, HREE), a signature that is difficult to achieve without fluorine- and boron-rich fluxing. Volatile saturation also fostered lower temperature and low-fO₂ conditions in the pegmatite, shifting redox equilibria to stabilize Mn^{2+} relative to Fe^{2+}/Fe^{3+} [59]. This explains the marked Mn enrichment and Fe depletion in pegmatitic CGMs, an imprint of crystallization in the presence of ferrous-iron-buffering volatiles (and possibly reduced species such as H_2 , CH_4) [24].

In parallel, structural controls provided the plumbing that focused metal-bearing melts and fluids into high-grade zones [58]. At the outcrop scale, Wadi Al-Baroud pegmatites occupy contacts with granites and are preferentially emplaced within intensely fractured domains. Such discontinuities, joints, faults, and lithologic boundaries likely channeled volatile-rich melts and hydrothermal fluids, concentrating pegmatite intrusion and subsequent fluid flow into specific corridors [12,15]. Textures support this where columbite lodged along healed fractures and interstitial sites in muscovite demonstrates that late fluids infiltrated micro-cracks and precipitated CGMs within those newly created voids. Moreover, the pervasive fracturing and metamictization in minerals such as euxenite implies that post-magmatic processes (e.g., metasomatism along cracks, radiation-damage-induced expansion) could further remobilize elements at the micro-scale, generating subtle redistribution into rims and alteration halos.

4.6. Comparison of Wadi Al-Baroud with Global Rare-Metal Pegmatite Systems

The evolutionary trends, mineralogical characteristics, and geochemical fingerprints documented at Wadi Al-Baroud closely parallel those of rare-metal granite-pegmatite systems worldwide, particularly within the lithium-cesium-tantalum (LCT) family. A combination of extreme fractional crystallization, fluorine enrichment, and Mn-Ta-HREE substitution, hallmarks of highly evolved rare-metal systems, are strikingly evident at Wadi Al-Baroud. For example, the Nb-Ta-Mn-Fe compositional trends observed in CGMs are analogous to those described from classical LCT pegmatite provinces such as the Preissac-Lacorne batholith in Quebec [40] and the P-F-rich pegmatites of Rwanda [56]. In these global examples, early columbite-(Fe) progressively evolves into manganotantalite as the melt becomes increasingly flux-rich and Ta-saturated, a pattern mirrored in Wadi Al-Baroud. The compositional overlap between Wadi Al-Baroud CGMs and those from the Julianna pegmatites in Poland [49] and the Little Nahanni LCT pegmatites of northwestern Canada [9] further supports this parallel evolution. The occurrence of Y-rich Nb-Ta mineral phase as an intermediate phase, also documented in Polish pegmatites [49], illustrates a

Minerals 2025, 15, 1206 18 of 22

common feature of large pegmatite bodies where internal zoning and melt entrapment lead to distinct mineralogical assemblages during different stages of evolution.

Fluorine-controlled REE partitioning at Wadi Al-Baroud exhibits additional global analogs. The pronounced LREE depletion and HREE enrichment of the euxenite, expressed by high Y/Dy ratios, are similar to observations from the Julianna pegmatite [49], though the latter displays lower Y/Dy values indicative of reduced fluorine availability. The exceptionally high Y/Dy ratios and HREE-rich oxide assemblages at Wadi Al-Baroud closely resemble those from the Varuträsk pegmatite in Sweden [60], a classic example of Y–HREE oxide mineralization in F-rich environments. Likewise, the distinctive convexupward HREE patterns of fergusonite-(Y) (Figure 6d) at Wadi Al-Baroud match those seen globally, such as in the Keivy alkaline granite, Russia [46], and the Abu Dob pegmatite, Egypt [61]. Slight negative Tm and Lu anomalies, attributed to size-selective incorporation into the Y–HREE oxide structure, further reinforce the similarity.

Structural influences on mineralization at Wadi Al-Baroud also parallel global observations. In the Chinese Altai pegmatite field, CGMs are commonly aligned along deformation zones within muscovite and feldspar [24], similar to the deformation-assisted emplacement seen in Wadi Al-Baroud. Likewise, many Nigerian [62] and Congolese [58] pegmatites host their most enriched Ta–Nb ores within shear zones and fractures, emphasizing the significance of structural heterogeneities in focusing late-stage mineralizing fluids. The tectonic context of Wadi Al-Baroud, emplacement along batholithic contacts in a post-collisional extensional area, is also characteristic of many fertile pegmatite provinces, including those in the Eastern Desert of Egypt and the Arabian Shield.

5. Conclusions

The mineralogical and geochemical characteristics of the Wadi Al-Baroud granite pegmatite system collectively document a complex history of rare-metal enrichment driven by extreme fractional crystallization, volatile-rich differentiation, and structural controls. The contrasting chemical signatures of CGMs in granite versus pegmatite highlight divergent evolutionary paths: granitic CGMs are Nb-rich, Mn-dominant, and relatively less evolved, whereas pegmatitic CGMs are Ta-, Fe-, and HREE-enriched, recording crystallization from a more fractionated, F- and H₂O-rich melt. The presence of a Y-rich Nb-Ta mineral phase underscores internal melt heterogeneity, marking intermediate stages of Nb depletion and incipient Ta accumulation. Late-stage Y-Nb-Ti oxides (fergusonite, euxenite) further demonstrate the role of fluorine in complexing HFSEs and HREEs, enabling their concentration in the final residual melt. Volatile activity, especially fluorine, emerges as the central driver of rare-metal enrichment by lowering melt viscosity, extending crystallization, and enhancing solubility of HFSEs and REEs. Simultaneously, structural discontinuities provided pathways and traps that localized mineralization, evident in the fracture-controlled emplacement of CGMs and the microtextural association of Nb-Ta oxides with muscovite. Thus, Wadi Al-Baroud records the interplay of magmatic, hydrothermal, and tectonic processes in shaping its rare-metal mineral assemblages. Wadi Al-Baroud exhibits the hallmarks of lithium-cesium-tantalum (LCT) pegmatites worldwide, including Nb→Ta fractionation trends, Mn-Fe-Ta substitutions, F-rich micas, and HREE-bearing Y oxides. Its mineralogical and geochemical signatures parallel those from major rare-metal districts in Canada, Poland, Rwanda, and the ANS, situating it firmly within the universal petrogenetic framework of highly evolved granite-pegmatite systems.

Minerals 2025, 15, 1206 19 of 22

Supplementary Materials: The following supporting information can be downloaded at: https://www.mdpi.com/article/10.3390/min15111206/s1.

Author Contributions: Conceptualization, M.S., I.V.S., M.R.A. and S.S.A.; methodology, M.S.; software, M.S. and V.D.K.; validation, M.S., I.V.S., M.R.A. and S.S.A.; formal analysis, M.S.; investigation, M.S., I.V.S., A.A.K., M.R.A., V.D.K. and S.S.A.; resources, M.S.; data curation, M.S., I.V.S., A.A.K., M.R.A., V.D.K. and S.S.A.; writing—original draft preparation, M.S. and V.D.K.; writing—review and editing, M.S., I.V.S., M.R.A. and S.S.A.; visualization, M.S., I.V.S., A.A.K., V.D.K. and S.S.A.; supervision, M.S.; project administration, M.S. and S.S.A.; funding acquisition M.S., I.V.S. and S.S.A. All authors have read and agreed to the published version of the manuscript.

Funding: Projects numbers (G00004879-12S155; Start-Up) and (G00004980-12S218; UPAR) from United Arab Emirates University, UAE and fund number (ORF-2025-1459; King Saud University, Saudi Arabia).

Data Availability Statement: All data derived from this research are presented in the enclosed figures and Supplementary Tables S1–S4.

Acknowledgments: The authors would like to express their appreciation to Theodoros Ntaflos and Franz Kiraly for assistance with the electron microprobe and the staff and technicians of the Department of Lithospheric Research, University of Vienna, Austria. Mabrouk Sami is grateful to Nasser M. Mahdy, Nuclear Materials Authority of Egypt for providing the samples. This study was financially supported by the grants (No G00004879-12S155 and G00004980-12S218) from the United Arab Emirates University, UAE. Sincere thanks and gratitude to the Ongoing Research Funding Program (ORF-2025-1459), King Saud University, Riyadh, Saudi Arabia, for funding this research article.

Conflicts of Interest: The authors declare no conflict of interest.

References

- 1. Elsagheer, M.A.; Azer, M.K.; Moussa, H.E.; Maurice, A.E.; Sami, M.; El Maaty, M.A.A.; Akarish, A.I.; Heikal, M.T.S.; Khedr, M.Z.; Elnazer, A.A. Late Neoproterozoic Rare-Metal Pegmatites with Mixed NYF-LCT Features: A Case Study from the Egyptian Nubian Shield. *Minerals* 2025, 15, 495. [CrossRef]
- 2. El Saeed, R.L.; Abart, R.; Ahmed, M.S.; Abdelfadil, K.M.; Farahat, E.S.; Sami, M. Petrological constraints of the Ediacaran magmatic intrusions, Homrit Mukpid area, southeastern Desert, Egypt: Bulk rock geochemistry and mineralogy. *J. Afr. Earth Sci.* 2025, 225, 105567. [CrossRef]
- 3. Sami, M.; Osman, H.; Ahmed, A.F.; Zaky, K.S.; Abart, R.; Sanislav, I.V.; Abdelrahman, K.; Fnais, M.S.; Xiao, W.; Abbas, H. Magmatic Evolution and Rare Metal Mineralization in Mount El-Sibai Peralkaline Granites, Central Eastern Desert, Egypt: Insights from Whole-Rock Geochemistry and Mineral Chemistry Data. *Minerals* 2023, 13, 1039. [CrossRef]
- 4. von Knorring, O.; Fadipe, A. On the mineralogy and geochemistry of niobium and tantalum in some granite pegmatites and alkali granites of Africa. *Bull. Minéralogie* **1981**, *104*, 496–507. [CrossRef]
- 5. Melcher, F.; Graupner, T.; Gäbler, H.E.; Sitnikova, M.; Henjes-Kunst, F.; Oberthür, T.; Gerdes, A.; Dewaele, S. Tantalum–(niobium–tin) mineralisation in African pegmatites and rare metal granites: Constraints from Ta–Nb oxide mineralogy, geochemistry and U–Pb geochronology. *Ore Geol. Rev.* **2015**, *64*, *667*–719. [CrossRef]
- 6. Khedr, M.Z.; Abo Khashaba, S.M.; Takazawa, E.; Hassan, S.M.; Azer, M.K.; El-Shibiny, N.; Abdelrahman, K.; Ichiyama, Y. Genesis of rare metal granites in the Nubian shield: Tectonic control and magmatic and metasomatic processes. *Minerals* **2024**, *14*, 522. [CrossRef]
- 7. Küster, D. Granitoid-hosted Ta mineralization in the Arabian–Nubian Shield: Ore deposit types, tectono-metallogenetic setting and petrogenetic framework. *Ore Geol. Rev.* **2009**, *35*, 68–86. [CrossRef]
- 8. Sami, M.; El Monsef, M.A.; Abart, R.; Toksoy-Köksal, F.; Abdelfadil, K.M. Unraveling the Genesis of Highly Fractionated Rare-Metal Granites in the Nubian Shield via the Rare-Earth Elements Tetrad Effect, Sr–Nd Isotope Systematics, and Mineral Chemistry. ACS Earth Space Chem. 2022, 6, 2368–2384. [CrossRef]
- 9. Groat, L.A.; Mulja, T.; Mauthner, M.H.; Ercit, T.S.; Raudsepp, M.; Gault, R.A.; Rollo, H.A. Geology and mineralogy of the Little Nahanni rare-element granitic pegmatites, Northwest Territories. *Can. Mineral.* **2003**, *41*, 139–160. [CrossRef]
- 10. Alfonso, P.; Hamid, S.A.; Garcia-Valles, M.; Llorens, T.; López Moro, F.J.; Tomasa, O.; Calvo, D.; Guasch, E.; Anticoi, H.; Oliva, J.; et al. Textural and mineral-chemistry constraints on columbite-group minerals in the Penouta deposit: Evidence from magmatic and fluid-related processes. *Miner. Mag.* 2018, 82, S199–S222. [CrossRef]

Minerals 2025, 15, 1206 20 of 22

11. Fawzy, M.M.; Mahdy, N.M.; Sami, M. Mineralogical characterization and physical upgrading of radioactive and rare metal minerals from Wadi Al-Baroud granitic pegmatite at the Central Eastern Desert of Egypt. *Arab. J. Geosci.* 2020, *13*, 413. [CrossRef]

- 12. Mahdy, N.M. Textural and chemical characteristics of zircon, monazite, and thorite, Wadi Al-Baroud area, Eastern Desert of Egypt: Implication for rare metal pegmatite genesis. *Ore Geol. Rev.* **2021**, *136*, 104225. [CrossRef]
- 13. Abd El Monsef, M.; Sami, M.; Toksoy-Köksal, F.; Abart, R.; Ondrejka, M.; Abdelfadil, K.M. Role of magmatism and related-exsolved fluids during Ta-Nb-Sn concentration in the Central Eastern Desert of Egypt: Evidences from mineral chemistry and fluid inclusions. *J. Earth Sci.* **2023**, *34*, 674–689. [CrossRef]
- 14. Azer, M.K.; Surour, A.A.; Moussa, H.E.; Maurice, A.E.; Sami, M.; Abou El Maaty, M.A.; Akarish, A.I.; Heikal, M.T.S.; Elnazer, A.A.; Elsagheer, M.A. Homrit Akarem Post-Collisional Intrusion, Southeastern Desert, Egypt: Petrogenesis of Greisen Formed in a Cupola Structure and Enrichment in Strategic Minerals. *Geosciences* 2025, *15*, 200. [CrossRef]
- 15. Abuamarah, B.A.; Alzahrani, H.; Matta, M.J.; Azer, M.K.; Asimow, P.D.; Darwish, M.H. Petrological, geochemical and geodynamic evolution of the Wadi Al-Baroud granitoids, north Arabian-Nubian shield, Egypt. J. Afr. Earth Sci. 2023, 207, 105044. [CrossRef]
- 16. Mohamed, F.R.; Hassan, E.E.S.; Sayed, A.O.; Ahmed, M.D. Mineralogy of polymetallic mineralized pegmatite of Ras Baroud granite, Central Eastern Desert, Egypt. *J. Mineral. Petrol. Sci.* **2010**, *105*, 123–134. [CrossRef]
- 17. Abdelfadil, K.M.; Semary, H.E.; Asran, A.M.; Rehman, H.U.; Sami, M.; Aldukeel, A.; Mogahed, M.M. Post-Collisional Mantle Processes and Magma Evolution of the El Bola Mafic–Ultramafic Intrusion, Arabian-Nubian Shield, Egypt. *Minerals* 2025, 15, 705. [CrossRef]
- 18. Abdelfadil, K.M.; Asran, A.M.; Rehman, H.U.; Sami, M.; Ahmed, A.; Sanislav, I.V.; Fnais, M.S.; Mogahed, M.M. The Evolution of Neoproterozoic Mantle Peridotites Beneath the Arabian–Nubian Shield: Evidence from Wadi Sodmein Serpentinites, Central Eastern Desert, Egypt. *Minerals* 2024, 14, 1157. [CrossRef]
- 19. Sami, M.; Azer, M.; Abdel-Karim, A.A. Postcollisional Ferani Volcanics from North Arabian–Nubian Shield (South Sinai, Egypt): Petrogenesis and Implication for Ediacaran (607–593 Ma) Geodynamic Evolution. *J. Geol.* **2022**, *130*, 475–498. [CrossRef]
- El-Dokouny, H.A.; Mahdy, N.M.; El Hadek, H.H.; Sami, M.; Abart, R.; Ahmed, M.S.; Zafar, T.; Sanislav, I.V. Origin of Amphibole-Biotite-Fluorite-Rich Enclaves from Gabal El-Ineigi Fluorite-Bearing Granite, Central Eastern Desert of Egypt: Insights into Fluoride-Calcium and Silicate Liquid Immiscibility. *Minerals* 2023, 13, 670. [CrossRef]
- 21. Abdel Monsif, M.; El Nahas, H.A.; Abdallah, S.M. Mineralogy and trace elements geochemistry of pegmatite body at the northern periphery of Gabal Ras Baroud, Central Eastern Desert, Egypt. *Nucl. Sci. Sci. J.* **2018**, *7*, 151–164. [CrossRef]
- 22. Miller, C.F.; Stoddard, E.F.; Bradfish, L.J.; Dollase, W.A. Composition of Plutonic Muscovite: Genetic Implications. *Can. Miner.* **1981**, *19*, 25–34.
- 23. Ryznar, J.; Pršek, J.; Włodek, A.; Uher, P. Mineralogy and chemistry of columbite-tantalite from Bugarura-Kuluti area, Karagwe-Ankole Belt, Rwanda: Indicators of pegmatite and granite evolution. *Ore Geol. Rev.* **2023**, *159*, 105574. [CrossRef]
- 24. Zhou, Q.; Qin, K.; Tang, D. Types and Evolution of Columbite-Group Minerals from Pegmatites in the Chinese Altai, NW China: Implications for Regional Petrogenesis and Rare-Element Mineralization. *Can. J. Mineral. Petrol.* **2024**, *62*, 317–351. [CrossRef]
- 25. Sallet, R.; Price, J.D.; Ribeiro, C.; Hollanda, M.H.B.; Sayeg, I.J.; Harlov, D. Fluorine behavior during experimental muscovite dehydration melting and natural partitioning between micas: Implications for the petrogenesis of peraluminous leucogranites and pegmatites. *Am. Mineral.* 2023, 108, 1201–1212. [CrossRef]
- 26. Clarke, D.B. The mineralogy of peraluminous granites; a review. Can. Mineral. 1981, 19, 3–17.
- 27. Koopmans, L.; Martins, T.; Linnen, R.; Gardiner, N.J.; Breasley, C.M.; Palin, R.M.; Groat, L.A.; Silva, D.; Robb, L.J. The formation of lithium-rich pegmatites through multi-stage melting. *Geology* **2023**, *52*, 7–11. [CrossRef]
- 28. Dostal, J.; Gerel, O. Occurrences of niobium and tantalum mineralization in Mongolia. Minerals 2022, 12, 1529. [CrossRef]
- 29. Breasley, C.M.; Groat, L.A.; Martins, T.; Linnen, R.L.; Larson, K.P.; Henry, R.E. Mineralogy and petrology of the petalite-subtype Prof pegmatite, Revelstoke, British Columbia, Canada. *Miner. Mag.* **2024**, *88*, 698–720. [CrossRef]
- 30. Siachoque, A.; Garcia, R.; Vlach, S.R. Occurrence and composition of columbite-(Fe) in the reduced a-type desemborque pluton, graciosa province (s-se Brazil). *Minerals* **2020**, *10*, 411. [CrossRef]
- 31. Sosa, G.M.; Augsburger, M.S.; Pedregosa, J.C. Columbite-group minerals from rare-metal granitic pegmatites of the Sierra de San Luis, Argentina. *Eur. J. Mineral.* **2002**, *14*, 627–636. [CrossRef]
- 32. René, M.; Škoda, R. Nb-Ta-Ti oxides fractionation in rare-metal granites: Krásno-Horní Slavkov ore district, Czech Republic. Mineral. Petrol. 2011, 103, 37–48. [CrossRef]
- 33. Fuchsloch, W.C.; Nex, P.A.; Kinnaird, J.A. The geochemical evolution of Nb–Ta–Sn oxides from pegmatites of the Cape Cross–Uis pegmatite belt, Namibia. *Miner. Mag.* **2019**, *83*, 161–179. [CrossRef]
- 34. Novák, M.; Cerny, P.; Uher, P. Extreme variation and apparent reversal of Nb-Ta fractionation in columbite-group minerals from the Scheibengraben beryl-columbite granitic pegmatite, Maršíkov, Czech Republic. *Eur. J. Mineral.* **2003**, *15*, 565–574. [CrossRef]
- 35. Cerny, P.; Nemec, D. Pristine Vs Contaminated Trends in Nb,Ta-Oxide Minerals of the Jihlava Pegmatite District, Czech-Republic. Mineral. Petrol. 1995, 55, 117–129. [CrossRef]

Minerals **2025**, 15, 1206 21 of 22

36. Martins, T.N.; Lima, A.; Falster, A.U.; Simmons, W.B.; Noronha, F. Geochemical fractionation of Nb–Ta oxides in Li-bearing pegmatites from the Barroso–Alvão pegmatite field, northern Portugal. *Can. Mineral.* **2011**, *49*, 777–791. [CrossRef]

- 37. Ercit, T.S.; Wise, M.A.; Cerny, P. Compositional and structural systematics of the columbite group. *Am. Mineral.* **1995**, *80*, 613–619. [CrossRef]
- 38. Linnen, R.L. The solubility of Nb-Ta-Zr-Hf-W in granitic melts with Li and Li + F; constraints for mineralization in rare metal granites and pegmatites. *Econ. Geol.* **1998**, *93*, 1013–1025. [CrossRef]
- 39. Tindle, A.G.; Breaks, F.W. Columbite-tantalite mineral chemistry from rare-element granitic pegmatites: Separation Lakeh area, N.W. Ontario, Canada. *Mineral. Petrol.* **2000**, *70*, 165–198. [CrossRef]
- 40. Mulja, T.; WilliamsJones, A.E.; Martin, R.F.; Wood, S.A. Compositional variation and structural state of columbite-tantalite in rare-element granitic pegmatites of the Preissac-Lacorne batholith, Quebec, Canada. *Am. Mineral.* **1996**, *81*, 146–157. [CrossRef]
- 41. Černý, P.; Ercit, T.; Wise, M.A. The tantalite-tapiolite gap; natural assemblages versus experimental data. *Can. Mineral.* **1992**, *30*, 587–596.
- 42. Gramaccioli, C.M.; Diella, V.; Demartin, F. The role of fluoride complexes in REE geochemistry and the importance of 4f electrons; some examples in minerals. *Eur. J. Mineral.* **1999**, *11*, 983–992. [CrossRef]
- 43. Zozulya, D.R.; Skublov, S.G.; Levashova, E.V.; Lyalina, L.M. Characteristics of the unique Y-HREE-F-RICH pegmatite system revealed by zircon geochemistry: A case study from Mt. Ploskaya amazonite deposit, Kola Peninsula. *Mineralogy* **2025**, *11*, 43–63.
- 44. Galliski, M.Á.; Márquez-Zavalía, M.F.; Pagano, D.S. Metallogenesis of the Totoral LCT rare-element pegmatite district, San Luis, Argentina: A review. *J. South Am. Earth Sci.* **2019**, *90*, 423–439. [CrossRef]
- 45. Matta, M.G.; Azer, M.K.; Darwish, M.H. Rare metals bearing pegmatites in the Nubian Shield: A case study of Ras Al-Baroud area, Eastern Desert of Egypt. *New Val. Univ. J. Basic Appl. Sci.* **2024**, *2*, 18–31. [CrossRef]
- Zozulya, D.; Macdonald, R.; Bagiński, B.; Jokubauskas, P. Nb/Ta, Zr/Hf and REE fractionation in exotic pegmatite from the Keivy province, NW Russia, with implications for rare-metal mineralization in alkali feldspar granite systems. Ore Geol. Rev. 2022, 143, 104779. [CrossRef]
- 47. Ercit, T.S. Identification and alteration trends of granitic-pegmatite-hosted (Y,REE,U,Th)-(Nb,Ta,Ti) oxide minerals: A statistical approach. *Can. Miner.* **2005**, *43*, 1291–1303. [CrossRef]
- 48. Alekseev, V.I.; Sukhanova, K.G.; Marin, Y.B. Niobium Minerals As Indicators of a Genetic Link Between Tin-Bearing Zwitter and Lithium–Fluorine Granite of the Verkhneurmiysky Massif in the Amur River Region. *Geol. Ore Depos.* **2018**, *60*, 698–707. [CrossRef]
- 49. Szuszkiewicz, A.; Pieczka, A.; Szełęg, E.; Turniak, K.; Ilnicki, S.; Nejbert, K. The Euxenite-Group Minerals and Products of Their Alteration In The Hybrid Julianna Granitic Pegmatite, Piława GÓrna, Sudetes, Southwestern Poland. *Can. Mineral.* **2017**, *54*, 879–898. [CrossRef]
- 50. Ewing, R.C. The crystal chemistry of complex niobium and tantalum oxides. IV. The metamict state: Discussion. *Am. Mineral. J. Earth Planet. Mater.* **1975**, *60*, 728–733.
- 51. Gonçalves, A.O.; Melgarejo, J.C.; Alfonso, P.; Amores, S.; Paniagua, A.; Neto, A.B.; Morais, E.A.; Camprubí, A. The distribution of rare metals in the LCT pegmatites from the Giraúl Field, Angola. *Minerals* **2019**, *9*, 580. [CrossRef]
- 52. Bartels, A.; Behrens, H.; Holtz, F.; Schmidt, B.C.; Fechtelkord, M.; Knipping, J.; Crede, L.; Baasner, A.; Pukallus, N. The effect of fluorine, boron and phosphorus on the viscosity of pegmatite forming melts. *Chem. Geol.* **2013**, 346, 184–198. [CrossRef]
- 53. Černý, P.; Ercit, T.S. The classification of granitic pegmatites revisited. Can. Mineral. 2005, 43, 2005–2026. [CrossRef]
- 54. Heinrich, C.A.; Candela, P.A. Fluids and ore formation in the Earth's crust. In *Treatise on Geochemistry*, 2nd ed.; Elsevier: Amsterdam, The Netherlands, 2014; Volume 13, pp. 1–28.
- 55. Sami, M.; Ntaflos, T.; Farahat, E.S.; Mohamed, H.A.; Ahmed, A.F.; Hauzenberger, C. Mineralogical, geochemical and Sr-Nd isotopes characteristics of fluorite-bearing granites in the Northern Arabian-Nubian Shield, Egypt: Constraints on petrogenesis and evolution of their associated rare metal mineralization. *Ore Geol. Rev.* 2017, 88, 1–22. [CrossRef]
- 56. Araujo, F.P.; Hulsbosch, N.; Muchez, P. Paragenesis and precipitation stages of Nb-Ta-oxide minerals in phosphorus-rich rare-element pegmatites (Buranga dike, Rwanda). *Am. Mineral. J. Earth Planet. Mater.* **2023**, *108*, 277–296. [CrossRef]
- 57. Li, Z.X.; Zhang, S.B.; Zheng, Y.F.; Wu, S.T.; Li, W.C.; Sun, F.Y.; Liang, T. Mobilization and fractionation of HFSE and REE by high fluorine fluid of magmatic origin during the alteration of amphibolite. *Lithos* **2022**, *420*–*421*, 106701. [CrossRef]
- 58. Kalikone, C.; Borst, A.; Nahimana, L.; Nzolang, C.; Nimpagaritse, G.; Batumike, J.; Rumanya, R.; Kezimana, L.; Delvaux, D.; Dewaele, S. Pegmatite zonation and the use of muscovite as a geochemical indicator for tin-tantalum-tungsten mineralization: Case studies from the Kalehe and Idjwi areas, Democratic Republic of Congo. *J. Afr. Earth Sci.* 2023, 207, 105067. [CrossRef]
- 59. Beskin, S.; Marin, Y.B. Granite systems with rare-metal pegmatites. Geol. Ore Depos. 2020, 62, 554–563. [CrossRef]
- 60. Černý, P.; Chapman, R.; Ferreira, K.; Smeds, S.A. Geochemistry of oxide minerals of Nb, Ta, Sn, and Sb in the Varuträsk granitic pegmatite, Sweden: The case of an "anomalous" columbite-tantalite trend. *Am. Mineral.* **2004**, *89*, 505–518. [CrossRef]

Minerals **2025**, 15, 1206 22 of 22

61. Raslan, M.; Fawzy, M.M. Mineralogy and Physical Upgrading of Fergusonite-Y and Hf-Zircon in The Mineralized Pegmatite of Abu Dob Granite, Central Eastern Desert, Egypt. *Bull. Tabbin Inst. Metall. Stud. (TIMS)* **2018**, *107*, 52–65. [CrossRef]

62. Cao, L.; Chen, X.; Jiang, J.; Garba, A.A.; Li, H.; Chao, N.; Hu, P.; Lv, X. Geochronology of cassiterite in the Nassarawa-Keffi rare metal pegmatite belt, Nigeria: Tectonic linkages to the Gondwana-forming orogeny. *Ore Geol. Rev.* 2024, 175, 106339. [CrossRef]

Disclaimer/Publisher's Note: The statements, opinions and data contained in all publications are solely those of the individual author(s) and contributor(s) and not of MDPI and/or the editor(s). MDPI and/or the editor(s) disclaim responsibility for any injury to people or property resulting from any ideas, methods, instructions or products referred to in the content.